ACS APPLIED MATERIALS & INTERFACES

Subscriber access provided by UIC Library

Article

Graphene can wreak havoc with cell membranes

Marco Dallavalle, Matteo Calvaresi, Andrea Bottoni, Manuel Melle-Franco, and Francesco Zerbetto

ACS Appl. Mater. Interfaces, **Just Accepted Manuscript** • DOI: 10.1021/am508938u • Publication Date (Web): 04 Feb 2015

Downloaded from http://pubs.acs.org on February 10, 2015

Just Accepted

"Just Accepted" manuscripts have been peer-reviewed and accepted for publication. They are posted online prior to technical editing, formatting for publication and author proofing. The American Chemical Society provides "Just Accepted" as a free service to the research community to expedite the dissemination of scientific material as soon as possible after acceptance. "Just Accepted" manuscripts appear in full in PDF format accompanied by an HTML abstract. "Just Accepted" manuscripts have been fully peer reviewed, but should not be considered the official version of record. They are accessible to all readers and citable by the Digital Object Identifier (DOI®). "Just Accepted" is an optional service offered to authors. Therefore, the "Just Accepted" Web site may not include all articles that will be published in the journal. After a manuscript is technically edited and formatted, it will be removed from the "Just Accepted" Web site and published as an ASAP article. Note that technical editing may introduce minor changes to the manuscript text and/or graphics which could affect content, and all legal disclaimers and ethical guidelines that apply to the journal pertain. ACS cannot be held responsible for errors or consequences arising from the use of information contained in these "Just Accepted" manuscripts.

ACS Publications
High quality. High impact.

ACS Applied Materials & Interfaces is published by the American Chemical Society.
1155 Sixteenth Street N.W., Washington, DC 20036

Published by American Chemical Society. Copyright © American Chemical Society.
However, no copyright claim is made to original U.S. Government works, or works produced by employees of any Commonwealth realm Crown government in the course of their duties.

Graphene can wreak havoc with cell membranes

Marco Dallavalle,[†,∥] *Matteo Calvaresi,*[†,∥,*] *Andrea Bottoni,*[†] *Manuel Melle-Franco,*[‡] *Francesco Zerbetto*[†,*]

[†] Dipartimento di Chimica "G. Ciamician", Alma Mater Studiorum – Università di Bologna, via F. Selmi 2, 40126 Bologna, Italy

[‡] Departamento de Informática, Centro de Ciências e Tecnologias da Computação, Universidade do Minho, 4710-057 Braga, Portugal

KEYWORDS. graphene, membrane, nanotoxicity, flip-flop, dissipative particle dynamics

ABSTRACT. Molecular dynamics -coarse grained to the level of hydrophobic and hydrophilic interactions- shows that small hydrophobic graphene sheets pierce through the phospholipid membrane and navigate the double layer; intermediate size sheets, pierce the membrane only if a suitable geometric orientation is met; larger sheets lie mainly flat on the top of the bilayer where they wreak havoc with the membrane and create a patch of upturned phospholipids. The effect arises in order to maximize the interaction between hydrophobic moieties and is quantitatively explained in terms of flip-flops by the analysis of the simulations. Possible severe biological consequences are discussed.

INTRODUCTION

With the development of various forms of nanotechnology, there is a need to understand their hazardous effects. Graphene and its derivatives, in particular, have potential for a wide variety of biomedical applications.[1] Possible short and long-term adverse health impacts must be considered in the design of graphenes for drug delivery, tissue engineering, and sensing devices.[2-5] The relatively limited data available suggest that graphene materials can be either benign[6-8] or toxic to cells.[9-29]

A recently proposed set of rules for the use of graphenes entailed:[30] (1) use of small, individual graphene sheets that macrophages in the body can efficiently internalize and remove from the site of deposition; (2) use of hydrophilic, stable, colloidal dispersions of graphene sheets to minimize aggregation in vivo; and (3) use of excretable graphene material or chemically-modified graphene that can be degraded effectively.

It has been suggested that the biological response depends on the number of layers, lateral size, stiffness, hydrophobicity, surface functionalization, and, perhaps obviously, dose.[3,10-31] The hydrophobic surface area of graphene may produce significant interactions with membrane phospholipids either causing direct physical toxicity or causing indirect toxicity.[9-35]

Despite the common carbon composition, graphene differs remarkably from another allotrope of carbon, namely carbon nanotubes. Graphene sheets have a lower aspect ratio, larger surface area, and better dispersibility in most solvents than nanotubes. Importantly, graphenes are not fiber-shaped. Most of these features of graphene appear advantageous in terms of safety over inhomogeneous dispersions of fiber-shaped carbon nanotubes.[30]

The issue arises of how and why cellular uptake of graphene nanosheets depends on size, shape, elasticity and surface structure. It would be desirable to know the effect of the size on receptor-mediated endocytosis, the effect of elastic stiffness on cell-particle interactions, and if different geometrical patterns of ligands on a sheet can be designed to control the rates of uptake by the cells.[36] The cytotoxicity of graphene nanosheets is hypothesized to originate from direct interactions between graphene and bacteria cell membranes that cause serious physical damages to the membranes. Simulations can provide important information on the interaction between graphene sheets and lipid membranes. [20,21,32-35]

Molecular dynamics simulations showed that the graphene sheets can be hosted in the hydrophobic interior of biological membranes formed by amphiphilic phospholipid molecules.[32]

MD and coarse grain simulations revealed the uptake process of graphene in cellular membranes. The entry was initiated at corners or asperities that were abundant along the irregular edges of graphene materials. Local piercing by these sharp protrusions initiated propagation along the extended graphene edge to achieve full penetration.[20]

Dissipative particle dynamics simulations showed the role of size and edges in the translocation of graphene nanosheets across a lipid bilayer membrane. The permeation of small sheets was driven by trans-bilayer lateral pressure. For larger nanosheets, the translocation underwent a vesiculation process. Circular sheets with smooth edges showed faster translocation than square ones.[33] Another study demonstrated the effects of graphene thicknesses (single/multi-layered graphene), oxidation, and lipid coating on the graphene entry. Pristine and few-layered graphene nanosheets could spontaneously insert into the bilayer and reach the centre of the bilayer.[34] Alternatively, edge oxidized graphene nanosheets could pierce the bilayer to reach a final state that was located at the center of the bilayer or stood upwards across the

bilayer, depending on the degree of oxidation.[34] Graphenes covered by a low density of lipid molecules could still pierce into the bilayer, initiating by one of the bare corners.[34] However, piercing could be hindered if the whole body of graphene was fully encapsulated in a lipid micelle. In the latter case, cell entry required fusion of a graphene encapsulated micelle and the bilayer.[34]

Very recently, simulations provided a systematic study of the interactions of graphene nanosheets, characterized by various sizes and oxidization degrees, with a simple model of lipid bilayer membrane. The detailed translocation pathways of these materials across the cellular membrane was obtained together with a phase diagram in the space of oxidization degree and particle size.[35] More importantly, a new state of the graphene-membrane interaction was identified: a hemispheric vesicle superstructure was formed through the adhesion of graphene to the top surface of the membrane.[35]

In addition, the simulations allowed to explain some experimental results by identifying two main mechanisms for graphene toxicity: i) the sharpened edges of graphene nanosheets may act like 'blades', which can insert and cut through the cell membranes of bacteria;[20] ii) the graphene nanosheet can extract phospholipids from the bilayers and accumulate them on its own surfaces.[21] The disruptive extraction of phospholipid molecules, caused by strong pulling forces from the graphene nanosheet, eventually led to the loss of cell membrane integrity.

In this work, we focus on the unexplored effects of a graphene sheet of increasing size on the structure of the phospholipid double layer. Small hydrophobic graphene sheets easily pierce through the phospholipid membrane; intermediate size sheets pierce the membrane only if a suitable geometric orientation is met, while larger sheets adsorb on the top of the bilayer where they modify the membrane and create a patch of upturned phospholipids. Both a static and a

dynamic description of the system is provided. The final equilibrium configuration in the bilayer is expressed in terms of normalized free energy and by means of the phospholipids order parameter. The perturbation caused by the presence of the graphene sheet is quantified in term of phospholipid translocation (flip-flop).

COMPUTATIONAL DETAILS

While other descriptions are possible, for the present purposes, Dissipative Particle Dynamics, DPD, is a thermostat, and a clever one to boot.[37] It complies with Newton's laws and satisfies fluidodynamics. The cost to pay is two-fold. The first compromise is that a Brownian component is explicitly included in the description of the motion, as is the case in Langevin's dynamics. The second concession to practicality is the necessity to introduce a relationship between Brownian and dissipation components of the nanoparticles motion. Under these conditions the time step used in the integration of the equation of motions can be made (much) longer than that used in standard molecular dynamics. Long time-steps, however, can be of little or no use if the weight of a particle is small. Light particles, such as atoms, vibrate at a high frequency. A long time step may encompass several oscillations and therefore introduce great instability in the algorithm that integrates the equations of motion, regardless of the fact that the thermostat would allow its use. The use of the DPD thermostat becomes efficient with particles heavier than atoms, which entail low frequency motions. The coarse graining of the atomistic structure can be achieved in many different ways. The choice here, as in many DPD applications, is to use soft sphere potentials.[38] These potentials can be traced back to Hildebrand's theory of real solutions[39] or, to Flory-Huggins theory of polymers.[39] They describe hydrophilic and hydrophobic interactions, which are at the core of the interaction between graphenes and phospholipid bilayer membranes.

It is possible to consider them as the convolution of many particles (atoms) interacting with many other particles (atoms). Each one of the two sets of atoms are then represented by a single particle or bead. This coarse graining has an important consequence. In a van der Waals system, the attractive interaction is a function of r_{ij}^{-6} , with i and j the interacting atoms. In the many atoms interacting with many atoms picture, the total energy becomes $\sum_{\substack{i\in A \\ j\in B}} r_{ij}^{-6}$ with A and B the two moieties that become beads. If a sufficiently large number of atoms are present inside each moiety that becomes coarse grained, the sum can be replaced by an integral and the power of -6 becomes less negative.

This very qualitative description does not consider that every $r_{ij}^{-6}\, r_{ij}^{-6}$ has its own coefficient, but it should suffice to justify a (strong) departure from the van der Waals description. As the number of atoms represented by the beads changes, their overall interaction may be modified. The approach allows to reduce drastically the computer times. The gain is more than 4 orders of magnitude. In practice, the calculations can either be extended over longer times, or to larger systems, or can be repeated many times to acquire sufficient statistics, if needed. The momentum-conserving thermostat of DPD, along with the implementation of soft repulsive interactions and coarse graining, makes it possible to simulate 1) the formation of architectures with a morphology resulting from solvophobic interactions (micelles, vesicles, and membranes), and 2) the dynamics of colloidal particles (nanoparticles) and their mutual interactions[40-49]

The DPD model used in this work is based on the approach introduced by Groot and coworkers.[50,51] The equations of motion are integrated using a modified velocity–Verlet algorithm.[50] All calculations were carried out using the suite of program Culgi 4.0.[52]

DPD Parameters

In this study, a phospholipid molecule consists of three linearly connected hydrophilic beads (labeled with the letter H), representing the polar headgroup, to which two tails of six hydrophobic beads (labeled by the letter T) are jointed. The water particle is labeled by the letter W. The GS is described as a colloidal particle and the soft-core colloid is modeled as an aggregate of soft-core beads (labeled by the letter G), as originally proposed by Koelman and Hoogerbrugge.[53]

The interactions between any two particles in the solution are described by the parameters in Table 1. In the simulations, the bead density was set at $\rho = 3$. A cubic simulation box of dimension 32 r_c x 32 r_c x 32 r_c was used and periodic boundary conditions were applied.

The total number of beads was 98304. Each of the calculations was run for 2500000 steps using a time step of 0.05τ.

Table 1. Bead pair interaction parameters. Conservative force parameter a_{ij} in units of k_BT/r_c .

H = Headgroup bead; T = Tail bead; W = Water bead; G = Graphene bead

a_{ij}	**H**	**T**	**W**	**G**
H	25	50	35	50
T	50	25	75	30
W	35	75	25	75
G	50	30	75	25

Phospolipids are constructed by tying beads together using Hookean springs with the potential: U_2 (i, i+1) = 1/2 k_2 (| $r_{i,i+1}$ | - l_0)^2 where i, i+1 represents adjacent beads in the phospolipids. The

spring constant, k_2, and unstretched length, l_0 , are chosen so as to fix the average bond length to a desired value. Both parameters may be specified independently for each bead pair, allowing a bond strength to vary along its length. Chain stiffness is modeled by a three-body potential acting between adjacent bead triples in a chain, U_3 (i-1,i,i+1) $= k_3$ [1-cos ($\Phi - \Phi_0$)]

where the angle Φ is defined by the scalar product of the two bonds connecting beads i-1, i, and i, i+1. The bending constant, k_3, and preferred angle, Φ_0, may be specified independently for different bead triples.

Table 2. Hookean springs force constants.

Bond Pair	k_2	l_0
H H	128	0.5
H T	128	0.5
T T	128	0.5
Bead Triples	k_3	Φ_0
T T T	20	180
H T T	20	180

Transformation of DPD Units

For transformation of dimensionless DPD units into physical length and time scales, it is necessary to link simulations with experimental data. The center-to-center distance between polar head group (PH) layers in cellular membranes is typically in the range of 40 Å (30 Å hydrophobic core (HC) domain, plus 5+5 Å for each half of the PH domain). In DPD simulations

this value corresponds to 6.955 r_c, where r_c is the unit length in the DPD system. From the above equivalence we determine r_c = 5.75 Å.

Following Groot and Rabone[54] the physical time scale may be obtained from the comparison of the calculated diffusion constant of water beads, D_{calc} with the experimental value[55] D_{exp}=2.43 10^{-5} cm^2/s

$$\tau = \frac{N_m D_{calc} r_c^2}{D_{\exp}}$$

N_m is the number of water molecules forming a "water bead" and the estimated self-volume for a single water molecule is 30 $Å^3$. Since a cubic volume of size r_c^3 (190.1 $Å^3$) represents ρN_m water molecules, with ρ=3 being the number of DPD beads per cubic r_c^3 it follows that N_m=2.1.

The diffusivity of a DPD particle is a dimensionless parameter that characterizes the fluid. It may be regarded as the ratio between the time needed by the particle to diffuse out to a certain distance and the time necessary for the hydrodynamic interactions to reach steady state conditions over comparable distances.[50] The diffusion coefficient of each bead is obtained by calculating the mean square displacement according to[54]

$$D = \lim_{t\to\infty} \frac{1}{6t} \left\langle \left| r_i(t) - r_i(t=0) \right|^2 \right\rangle$$

The resulting value of D_{calc} = 0.31 substituted into the above equation yields a final DPD unit time of 88.6 ps.

The typical DPD simulation length of 2,500,000 steps, with a time step of 0.05τ that corresponds to a physical time of 11 μs.

RESULTS AND DISCUSSIONS

DPD calculations were carried out using a system composed of water, phospholipids and graphene nanosheets, GS, of different sizes. Figure 1 shows the coarse grained models for the representative entities used in the DPD simulations. A phospholipid is represented by three linearly connected hydrophilic soft beads that represent the polar headgroup, two tails of six hydrophobic soft beads join the polar head, following the Shillcock and Lipowsky model.[56] Amphiphiles possessing two hydrophobic tails require three or more head beads to shield the tails from the surrounding solvent, and form a well-ordered bilayer.[56] DPD parameters for the phospholipids were taken from the accurate model of Shillcock and Lipowsky[56] that is capable of reproducing the structural properties and the stress profile of bilayers. The stretch modulus and the bending rigidity of the membrane simulated with these parameters are comparable to experimental values for typical phospholipid bilayers.[56] For the complete discussion, please see Ref 56. Water particles are represented by a single bead.

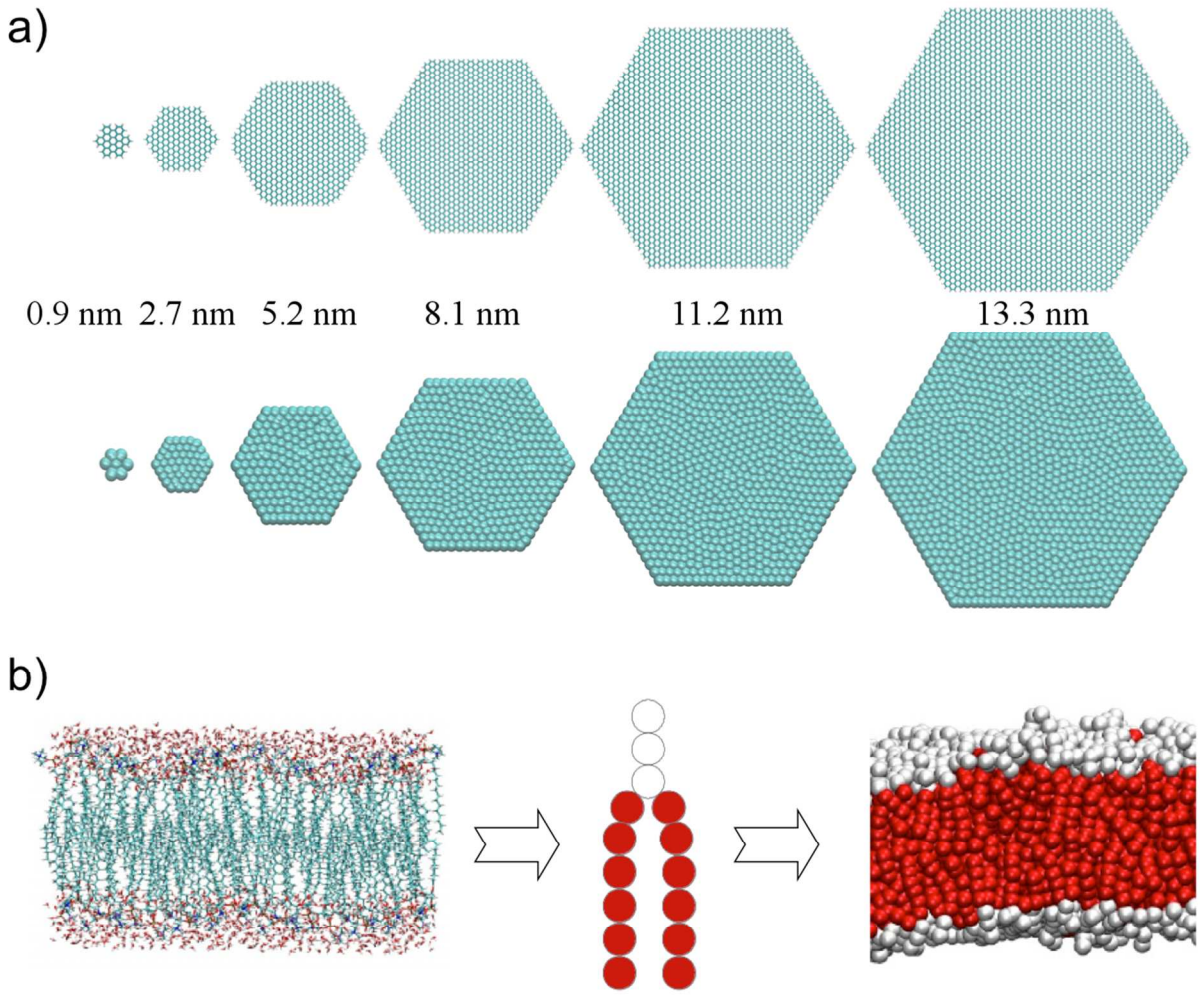

Figure 1. Description of coarse-grained molecular dynamics models for the representative entities used in the simulations. a) Coarse graining of the GS. b) Coarse graining of the membrane. The model of amphiphilic phospholipid is constructed by a head group with three hydrophilic beads (white) and two tails consisting of six hydrophobic beads (red).

For the GS we used a set of parameters developed by us to reproduce the experimental self-assembly of carbon nanomaterials with amphiphilic molecules.[40-43] DPD runs were repeated five times to acquire sufficient statistics. A self-assembled and equilibrated bilayer was present in the simulation box with every GS positioned randomly at five different starting position.

Figure 2 provides snapshots of the GS/phospholipid bilayer interaction at the end of the simulations. The particle size of the GS determined its final configuration in the bilayer. The five smaller sheets pierced through the membrane. The four larger sheets can adhered to the membrane, a deed that is not done by the two smaller sheets. Sheets smaller than 5.2 nm were also able to navigate the membrane (vide infra). Increasing their size and up to 11.2 nm, they crossed the bilayer only if a suitable geometric orientation was met and, correspondingly, two minima were found in the free energy surface (Figure 3). In the first minimum, the GS pierced through, in the second one it adsorbed on the membrane. If larger than 11.2 nm, the sheets were unable to cross the membrane. Assumptions are necessary when comparing experimental and MD results. The small size GS used in most experiments are larger than or similar to the largest sheets of the current MD study. We present an idealized system with a single graphene sheet where the formation of aggregates is neglected. Experiments are usually carried out with suspension of graphene derivatives. However, these results are in line with the size-dependency on GS cellular internalization process.[17,18,28,29,31,35]

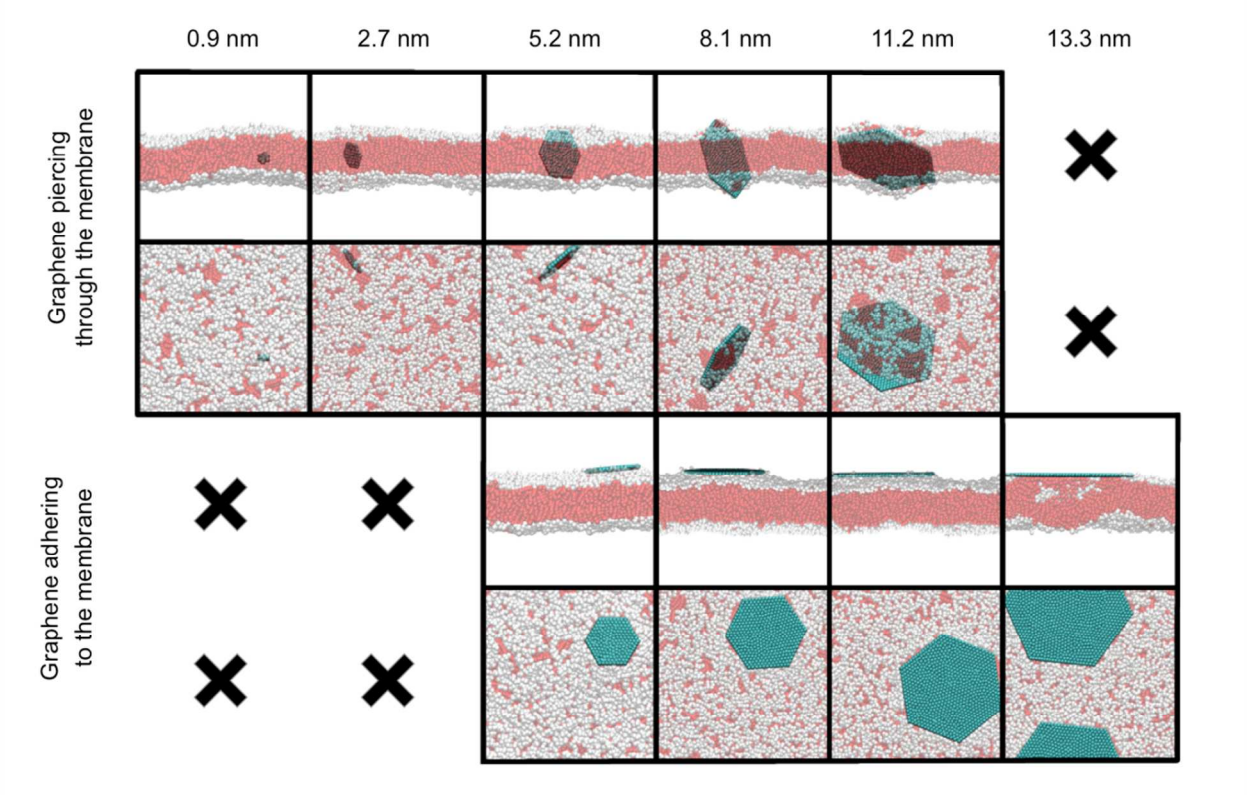

Figure 2. Illustrative snapshots, at the end of the simulations, of six graphene nanosheets of increasing size. From left to right, sizes of 0.9, 2.7, 5.2, 8.1, 11.2, and 13.3 nm. White: hydrophilic heads of the phospholipids; red: hydrophobic phospholipid tails; petroleum blue: graphenes. For clarity, water is not shown. Top two rows are different perspectives of the six sheets, as are the bottom two rows. Only the five smaller sheets pierce through the membrane. The four larger sheets adhere to the membrane. Situations not observed in the simulations are indicated by X.

The preferred orientation of the GS was also size dependent. In figures 3 the x-axis shows the angle of the sheet with the phospholipid bilayer. A value of the angle close to 0˚ means that the sheet was parallel to the membrane; a value close to 90˚ means that it was perpendicular to it.

The smaller the sheet, the more freely it diffused inside the membrane. Small sheets preferentially align with the phospholipid hydrophobic tails and maintained a perpendicular orientation. Sheets greater than the membrane thickness moved to smaller angles, arranged themselves across the membrane to be embedded as much as possible in the hydrophobic part of the bilayer. Even greater sheets only adhered to the external surface of the membrane.

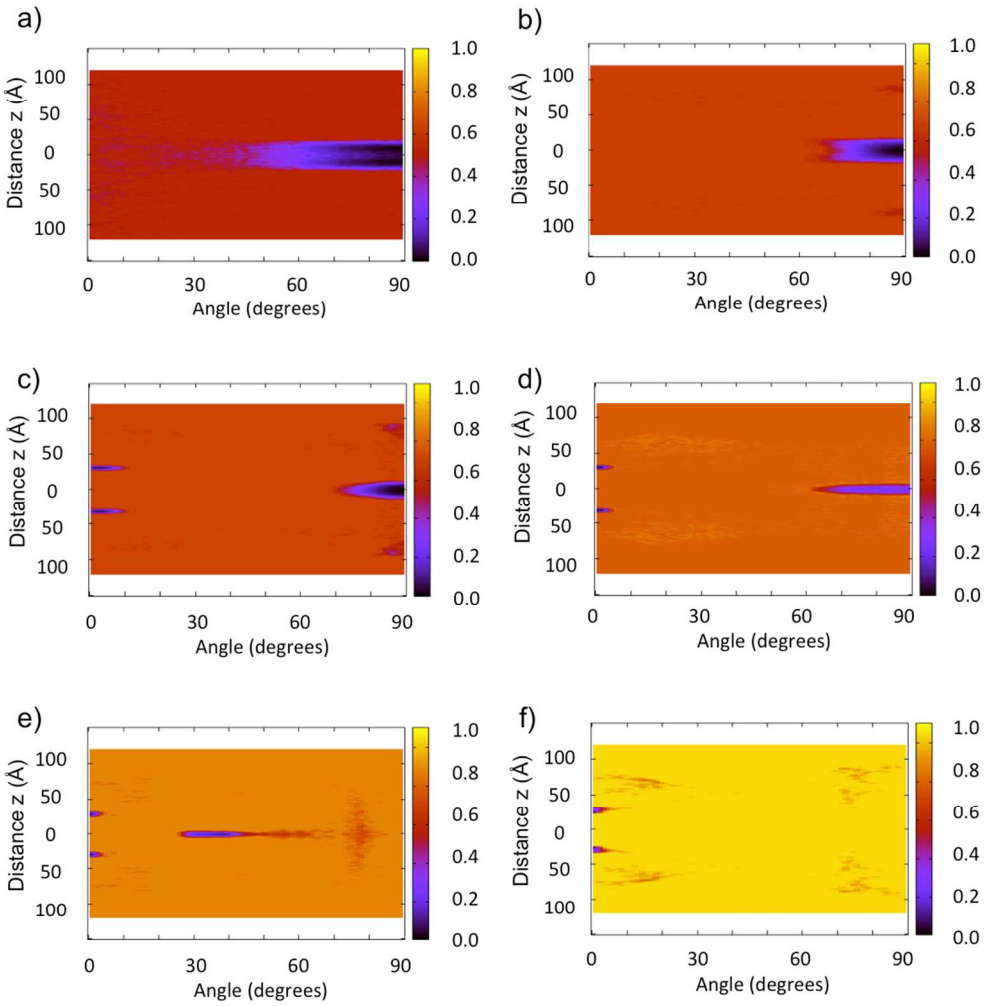

Figure 3. Normalized free energy of the systems as a function of the graphene penetration and orientation. Sheet sizes a) 0.9 nm, b) 2.7 nm, c) 5.2 nm, d) 8.1 nm, e) 11.2 nm and f) 13.3 nm.

The presence of the sheet affected the overall density distribution of the hydrophobic and hydrophilic moieties of the phospholipids. Figure 4 compares, the densities for the unperturbed membrane (Fig. 4a) and for the perturbed bilayer when the graphene flake (size 11.2 nm) pierced through (Fig. 4b) or adhered (Fig. 4c) to the membrane. When graphene penetrated the membrane (Fig 4b), some phospholipids stuck to graphene and followed GS movements (Fig. 5a). The head beads were no longer excluded from the bilayer interior and the two monolayers were not any longer properly interdigitated. When GS adsorbed on the membrane an asymmetry was induced in the membrane bilayer (Fig 4c) because the hydrophobic tail beads tended to move toward the interface with the GS nanoparticle (Fig 5b).

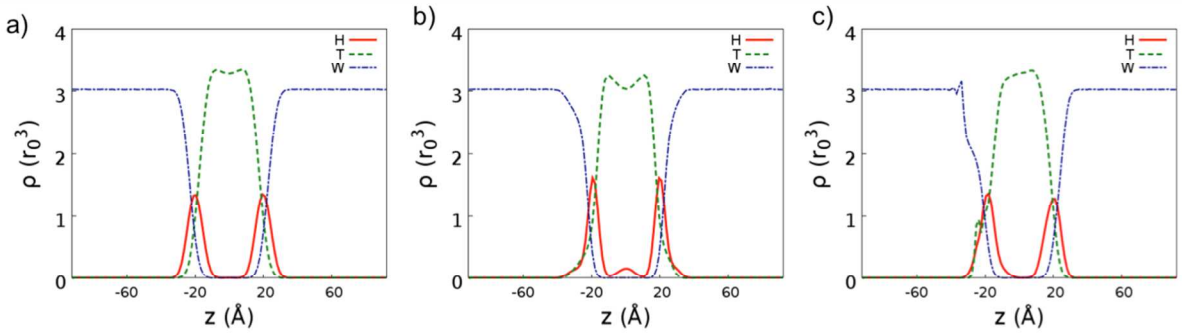

Figure 4. Density profiles of the phospholipid bilayers. Hydrophilic head beads, H, hydrophobic tail beads, T, bulk water, W (a) unperturbed membrane; (b) bilayer pierced by the graphene sheets (c) adhesion of the graphene to the membrane. The profiles were averaged over 1000 steps.

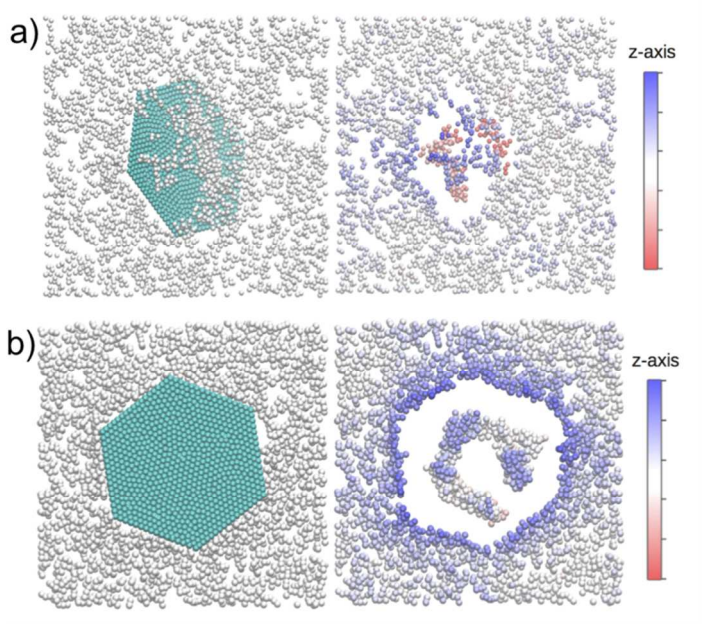

Figure 5. Two views of the interaction of GS with the membrane are depicted corresponding to a) piercing through, and b) adsorbing onto the membrane. The z-axis color code corresponds to the position of the phospholipids heads. The graphene flake locally affects the membrane structure. The empty spaces are occupied by the tails. Phospholipids are displaced with respect to the z-average position. Water molecules are not shown.

The order parameter, $S = \left\langle \frac{3}{2}\cos^2\theta - \frac{1}{2} \right\rangle$, allows a more quantitative evaluation of the orientational order (or disorder) induced by the sheets in the phospholipids of the membrane. The angle, θ, is formed by an axis perpendicular to the membrane and the long axis of each molecule. An unperturbed membrane is characterized by S=0.73. Table 3 compares the global (all the phospholipids are considered) and the local (only the phospholipids within the range of 1.5 r_c, roughly 8.6 Å, from the GS were considered) order parameters of the phospholipids, averaged over 100 steps of the equilibrated systems.

Table 3. Global versus local (dis-)order induced by graphene sheets piercing through or adhering to the membrane.

Nanosheet size (nm)	GS piercing through the membrane		GS adhering to the membrane	
	S_{local}	S_{global}	S_{local}	S_{global}
0.9	0.72	0.69	--	--
2.7	0.72	0.69	--	--
5.2	0.77	0.68	0.03	0.66
8.1	0.34	0.65	-0.16	0.59
11.2	0.10	0.57	-0.16	0.52
13.3	--	--	-0.13	0.45

Small GS piercing the membrane did not perturb, both globally and locally, the order of the membrane and could easily enter the cell. The higher cellular uptake for ultra-small GS[57] can be explored to make them ideal nanocarriers for drug delivery systems. Increasing the size of the GS (> 5.2 nm) strong local perturbations of the membrane were observed. The global order of the membrane was more or less maintained for piercing GSs. On the contrary, an adhering sheet induced a substantial disorder. Larger sheets induced local anti-alignment (S is negative for anti-alignment).

The question arises of whether the anti-alignment is related to the presence, in itself puzzling, of a hydrophobic GS that adheres to the top of a membrane, which is hydrophilic. Peeling off the nanosheet revealed that the phospholipids of the layer directly under the sheet capsized and interacted with the sheet with the hydrophobic tail (Figure 6). The anti-alignment was therefore truly related to the hydrophobic-hydrophobic interaction that allowed the sheet to adhere to the membrane. Importantly, the overturned phospholipids could impair cell functioning and disrupt

the functioning of the membrane proteins. They may explain the cytotoxic activity of adhering GSs, the so-called masking effect.[18,19,28] Experimentally availability of the basal planes of graphene determines whether it is cytotoxic.[27] Notice that size-dependent GS toxicity and changes in the toxicity mechanisms are well-known experimentally[17-20,28,29] and computationally.[20,33,35]

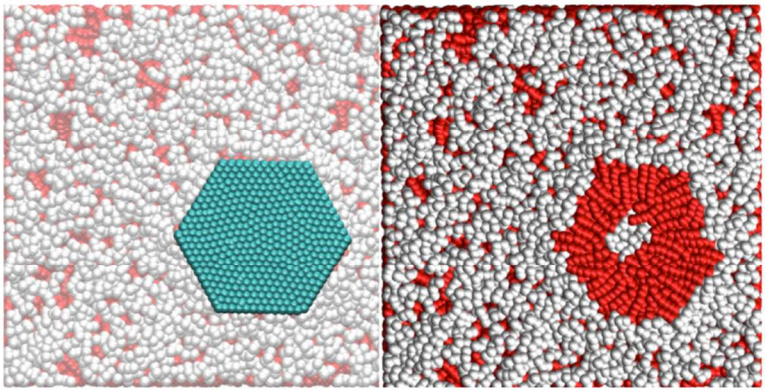

Figure 6. Left, a sheet adhering to the phospholipid membrane; right, peeling off the sheet shows that the hydrophobic tails directly interact with hydrophobic graphene.

The adsorption of the graphene flake triggered the translocation from one layer to the other of multiple phospholipids (Table 4). Liu et al. demonstrated that the migration of lipids in living cells could be facile under physiological conditions, also in the absence of a protein-mediated process, on the second timescale. In the presence of GS, the majority of translocation events occurred as soon as the graphene sheet settled on the top of the layer, figure 7, in less than a microsecond. During the rest of the dynamics the number of flip-flops remained constant, within statistical fluctuations.

Table 4. Average number, over five dynamics, of flip-flops during 11 microseconds of dynamics for different sheets sizes. An unperturbed membrane is characterized by an average number of translocation events equal to 3.

Nanosheet size (nm)	Number of translocation events
0.9	3
2.7	4
5.2	8
8.1	17
11.2	41
13.3	46

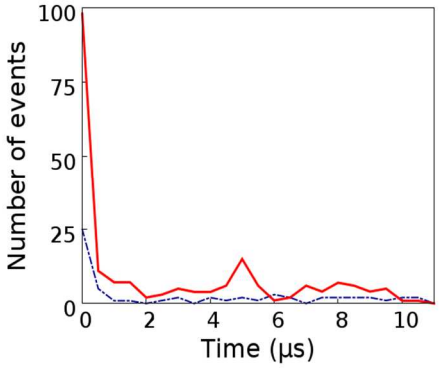

Figure 7. Phospholipid translocation for the largest GS: solid red line, the phospholipid drifts from the unperturbed leaflet to the graphene interface; dashed dotted blue line, the phospholipid wanders from the perturbed leaflet to the opposite layer.

The spontaneous translocation of a phospholipid in the membrane usually involves 3 steps (Figure 8a). In the first the phospholipid desorbs from a layer, in the second it re-orients itself, in the third it accommodates in the opposite layer.

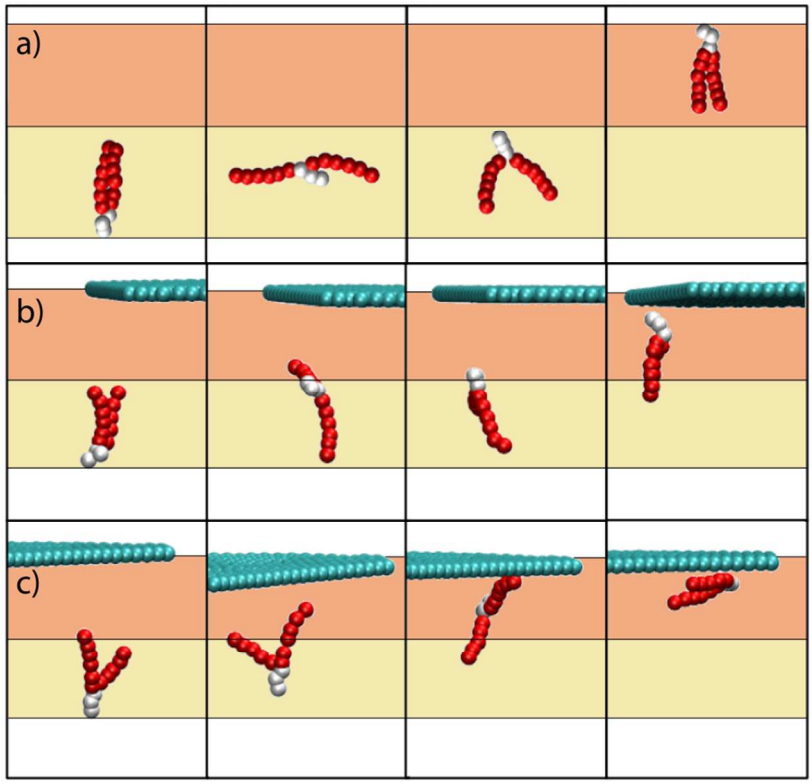

Figure 8. Spontaneous translocation of a phospholipid in the membrane. For sake of clarity, only the flip-flopping phospholipid and the graphene flake are shown. The two layers of the membrane are represented as continuous fields. a) Spontaneous translocation of a phospholipid in a membrane; b) translocation with re-orientation in the presence of a GS; c) translocation without re-orientation in the presence of a GS.

The largest GS is taken as a representative case. Only in the 34.8% of the cases (80 out of 46*5=230), the phospholipid reoriented in the starting layer and subsequently diffused to the opposite layer (Figure 8b). This mechanism was mostly observed when the translocating phospholipid was located at the interface with graphene. In 65.2% of the cases (150 out of 230), a new mechanism was observed. The phospholipid did not somersault and reached the opposite layer without reorienting. In more detail, the translocations observed during the dynamics

belonged to three types. The first type was the detachment of a phospholipid from the layer further away from the graphene sheet. The phospholipid subsequently accommodated itself in the other layer at the interface with the GS. The path started from the unperturbed region and reached the perturbed area. The second type followed the opposite path. There was a detachment of a phospholipid from the layer perturbed by the graphene sheet with its subsequent accommodation in the opposite layer. The third type of translocation was the reversible accommodation of a phospholipid at the graphene interface. The phospholipid desorbed from the unperturbed layer, travelled to the opposite one and then drifted back to the initial membrane.

The percentage of events of the first type was 74.3 % (171 out of 230); of the second type was 11.3% (26 out of 230); of the third type was 14.3% (33 out of 230). The global motion of the phospholipids, induced by the GS, generated an asymmetric density distribution (Figure 4c). The layer closer to the graphene sheet was enriched by the translocations, while the layer further away was impoverished. Biologically, translocation of phospholipids to the external side of the membrane triggers a number of membrane associated events, including recognition and elimination of apoptotic or aged cells.[59] Apoptosis in macrophages can be triggered by pristine graphene.[60] The translocation mechanism discussed here can also modify the polarization of the cellular membrane and induce cytotoxicity.

CONCLUSION

Some of the properties of carbon nanoparticles and graphene in particular bear on biomolecular[61-70] and cellular interactions.[11-31] We have shown how different graphene sheets navigate different regions of the phospholipid bilayer and its surroundings and we have quantitatively investigated the re-organization of the bilayer induced by the presence of larger sheets. Small sheets entered the membrane without affecting the order of the phospholipids. Larger sheets adsorbed on its top strongly affecting the order and to a lesser, but noteworthy extent, the density and the distribution of the phospholipids. The most common type of events induced by a GS was the translocation of phospholipids that occurred from the unperturbed layer to the perturbed one without inversion of polarity. The insertion of new phospholipids formed a patch of upturned molecules with their hydrophobic tail interacting directly with the hydrophobic graphene sheet. These events could induce cytotoxicity by modifying the membrane polarization and trigger apoptosis by externalization of phospholipids.

AUTHOR INFORMATION

Corresponding Author

* MC: matteo.calvaresi3@unibo.it; FZ: francesco.zerbetto@unibo.it

Author Contributions

The manuscript was written through contributions of all authors. ‖These authors contributed equally.

REFERENCES

(1) Kostarelos, K.; Novoselov, K. S. Exploring the Interface of Graphene and Biology. *Science* **2014***, 344*, 261-263.

(2) Feng, L.; Liu, Z. Graphene in Biomedicine: Opportunities and Challenges. *Nanomedicine*, **2011**, *6*, 317-324.

(3) Sanchez, V. C.; Jachak, A.; Hurt, R. H.; Kane, A. B. Biological Interactions of Graphene-Family Nanomaterials: An Interdisciplinary Review. *Chem. Res. Toxicol.* **2012**, 25, 15-34.

(4) Nguyen, P.; Berry, V. Graphene Interfaced with Biological Cells: Opportunities and Challenges. *J. Phys. Chem. Lett.* **2012**, *3*, 1024-1029.

(5) Zhang, Y.; Nayak, T. R.; Hong, H.; Cai, W. B. Graphene: A Versatile Nanoplatform for Biomedical Applications. *Nanoscale* **2012**, *4*, 3833-3842.

(6) Cha, C.; Shin, S. R.; Annabi, N.; Dokmeci, M. R.; Khademhosseini, A. Carbon-Based Nanomaterials: Multifunctional Materials for Biomedical Engineering. *ACS Nano*, **2013**, *7*, 2891-2897.

(7) Chung, C.; Kim, Y.-K.; Shin, D.; Ryoo, S.-R.; Hong, B. H.; Min, D.-H. Biomedical Applications of Graphene and Graphene Oxide. *Acc. Chem. Res.* **2013**, *46*, 2211-2224.

(8) Servant, A.; Bianco, A.; Prato, M.; Kostarelos, K. Graphene for Multi-Functional Synthetic Biology: The Last 'Zeitgeist' in Nanomedicine. *Bioorg. Med. Chem. Lett.* **2014**, *24*, 1638-1649.

(9) Zhou, R.; Gao, H. Cytotoxicity of Graphene: Recent Advances and Future Perspective. *Wires Nanomed. Nanobi.* **2014**, *6*, 452-474.

(10) Bianco, A. Graphene: Safe or Toxic? The Two Faces of the Medal. *Angew. Chem. Int. Ed.* **2013**, *52*, 4986-4997.

(11) Hu, W.; Peng, C.; Luo, W.; Lv, M.; LiX,Li, D.; Huang, Q.; Fan, C. Graphene-Based Antibacterial Paper. *ACS Nano* **2010**, *4*, 4317-4323.

(12) Akhavan, O.; Ghaderi, E. Toxicity of Graphene and Graphene Oxide Nanowalls Against Bacteria. *ACS Nano* **2010**, *4*, 5731-5736.

(13) Zhang, Y.; Ali, S. F.; Dervishi, E.; Xu, Y.; Li, Z.; Casciano, D.; Biris, A. S. Cytotoxicity Effects of Graphene and Single-Wall Carbon Nanotubes in Neural Phaeochromocytoma-Derived PC12 Cells. *ACS Nano* **2010**, *4*, 3181-3186.

(14) Liao, K.-H.; Lin, Y.-S.; Macosko, C. W.; Haynes, C. L. Cytotoxicity of Graphene Oxide and Graphene in Human Erythrocytes and Skin Fibroblasts. *ACS Appl. Mater. Interfaces* **2011**, *3*, 2607–2615.

(15) Liu, S.; Zeng, T. H.; Hofmann, M.; Burcombe, E.; Wei, J.; Jiang, R.; Kong, J.; Chen, Y. Antibacterial Activity of Graphite, Graphite Oxide, Graphene Oxide, and Reduced Graphene Oxide: Membrane and Oxidative Stress. *ACS Nano* **2011**, *5*, 6971-6980.

(16) Sasidharan, A.; Panchakarla, L. S.; Chandran, P.; Menon, D.; Nair, S.; Rao, C. N. R.; Koyakutty, M. Differential Nano-Bio Interactions and Toxicity Effects of Pristine Versus Functionalized Graphene. *Nanoscale* **2011**, *3*, 2461-2464.

(17) Akhavan, O.; Ghaderi, E.; Akhavan, A. Size-Dependent Genotoxicity of Graphene Nanoplatelets in Human Stem Cells. *Biomaterials* **2012**, *33*, 8017-8025.

(18) Liu, S.; Hu, M.; Zeng, T. H.; Wu, R.; Jiang, R.; Wei, J.; Wang, L.; Kong, J.; Chen, Y. Dimension-Dependent Antibacterial Activity of Graphene Oxide Sheets. *Langmuir* **2012**, *28*, 12364-12372.

(19) Russier, J.; Treossi, E.; Scarsi, A.; Perrozzi, F.; Dumortier, H.; Ottaviano, L.; Meneghetti, M.; Palermo, V.; Bianco, A. Evidencing the Mask Effect of Graphene Oxide: a Comparative Study on Primary Human and Murine Phagocytic Cells. *Nanoscale* **2013**, *5*, 11234-11247.

(20) Li, Y.; Yuan, H.; Von dem Bussche, A.; Creighton, M.; Hurt, R. H.; Kane, A. B.; Gao, H. Graphene Microsheets Enter Cells Through Spontaneous Membrane Penetration at Edge Asperities and Corner Sites. *Proc. Natl. Acad. Sci. USA* **2013**, *110*, 12295-12300.

(21) Tu, Y.; Lv, M.; Xiu, P.; Huynh, T.; Zhang, M.; Castelli, M.; Liu, Z.; Huang, Q.; Fan, C.; Fang, H.; Zhou, R. Destructive Extraction of Phospholipids from *Escherichia coli* Membranes by Graphene Nanosheets. *Nat. Nanotechnol.* **2013**, *8*, 594-601.

(22) Lammel, T.; Boisseaux, P.; Fernández-Cruz, M.-L.; Navas, J. M. Internalization and Cytotoxicity of Graphene Oxide and Carboxyl Graphene Nanoplatelets in the Human Hepatocellular Carcinoma Cell Line Hep G2. *Part. Fibre Toxicol.* **2013**, *10*, 27.

(23) Tang, J.; Chen, Q.; Xu, L.; Zhang, S.; Feng, L.; Cheng, L.; Xu, H.; Liu, Z.; Peng, R. Graphene Oxide−Silver Nanocomposite As a Highly Effective Antibacterial Agent with Species-Specific Mechanisms. *ACS Appl. Mater. Interfaces* **2013**, *5*, 3867-3874.

(24) Wang, T.-W.; Cao, A.; Jiang, Y.; Zhang, X.; Liu, J.-H.; Liu, Y.; Wang, H. Superior Antibacterial Activity of Zinc Oxide/Graphene Oxide Composites Originating from High Zinc Concentration Localized around Bacteria. *ACS Appl. Mater. Interfaces* **2014**, *6*, 2791-2798.

(25) Ding, Z.; Zhang, Z.; Ma, H.; Chen, Y. In Vitro Hemocompatibility and Toxic Mechanism of Graphene Oxide on Human Peripheral Blood T Lymphocytes and Serum Albumin. *ACS Appl. Mater. Interfaces* **2014**, *6*, 19797-19807.

(26) Linares, J.; Matesanz, M. C.; Vila, M.; Feito, M. J.; Goncąlves, G.; Vallet-Regí, M.; Marques, P. A. A. P.; Portoleś, M. T. Endocytic Mechanisms of Graphene Oxide Nanosheets in Osteoblasts, Hepatocytes and Macrophages. *ACS Appl. Mater. Interfaces* **2014**, *6*, 13697-13706.

(27) Hui, L.; Piao, J.-G.; Auletta, J.; Hu, K.; Zhu, Y.; Meyer, T.; Liu, H.; Yang, L. Availability of the Basal Planes of Graphene Oxide Determines Whether It Is Antibacterial. *ACS Appl. Mater. Interfaces* **2014**, *6*, 13183-13190.

(28) Chang, Y.; Yang, S.-T.; Liu, J.-H.; Dong, E.; Wang, Y.; Cao, A.; Liu, Y.; Wang, H. In vitro Toxicity Evaluation of Graphene Oxide on A549 Cells. *Toxicol. Lett.* **2011**, *200*, 201-210.

(29) Liu, J.-H.; Yang, S.-T.; Wang, H., Chang, Y.; Cao, A.; Liu, Y. Effect of Size and Dose on the Biodistribution of Graphene Oxide in Mice. *Nanomedicine (Lond.)* **2012**, *7*, 1801-1812.

(30) Bussy, C.; Ali-Boucetta, H.; Kostarelos, K. Safety Considerations for Graphene: Lessons Learnt from Carbon Nanotubes *Acc. Chem. Res.* **2013**, *46*, 692-701.

(31) Mu, Q.; Su, G.; Li, L.; Gilbertson, B. O.; Yu, L. H.; Zhang, Q.; Sun, Y.-P.; Yan, B. Size-Dependent Cell Uptake of Protein-Coated Graphene Oxide Nanosheets. *ACS Appl. Mater. Interfaces* **2012**, *4*, 2259-2266.

(32) Titov, A. V.; Kral, P.; Pearson, R. Sandwiched Graphene-Membrane Superstructures. *ACS Nano* **2010**, *4*, 229-234.

(33) Guo, R.; Mao, J.; Yan, L.-T. Computer Simulation of Cell Entry of Graphene Nanosheet. *Biomaterials* **2013**, *34*, 4296-4301.

(34) Wang, J.; Wei, Y.; Shi, X.; Gao, H. Cellular Entry of Graphene Nanosheets: the Role of Thickness, Oxidation and Surface Adsorption. *RSC Adv.* **2013**, *3*, 15776-15782.

(35) Mao, J.; Guo, R.; Yan, L.-T. Simulation and Analysis of Cellular Internalization Pathways and Membrane Perturbation for Graphene Nanosheets. *Biomaterials* **2014**, *35*, 6069-6077.

(36) Gao, H. Probing Mechanical Principles of Cell-Nanomaterial Interactions. *J. Mech. Phys. Solids* **2014**, *62*, 312-339.

(37) Soddermann, T.; Dünweg, B.; Kremer, K. Dissipative Particle Dynamics: A Useful Thermostat for Equilibrium and Nonequilibrium Molecular Dynamics Simulations. *Phys. Rev. E*, **2003**, *68*, 046702.

(38) Hoogerbrugge, P. J.; Koelman, J. M. V. Simulating Microscopic Hydrodynamic Phenomena with Dissipative Particle Dynamics. *Europhys. Lett.* **1992**, *19*, 155.

(39) Prausnitz, J. M.; Lichtenthaler, de Azevedo, E. G. *Molecular Thermodynamics and Fluid-Phase Equilibria*. 2nd ed., Prentice-Hall inc., Englewood Cliffs, New Jersey, **1986**.

(40) Calvaresi, M.; Dallavalle, M.; Zerbetto F. Wrapping Nanotubes with Micelles, Hemimicelles, and Cylindrical Micelles. *Small* **2009**, *5*, 2191-2198.

(41) Höfinger, S.; Melle-Franco, M.; Gallo, T.; Cantelli, A.; Calvaresi, M.; Gomes, J. A. N. F.; Zerbetto, F. A Computational Analysis of the Insertion of Carbon Nanotubes into Cellular Membranes. *Biomaterials* **2011**, *32*, 7079-7085.

(42) Min, S. H.; Lee, C.; Jang, J. Dissipative Particle Dynamics Modeling of a Graphene Nanosheet and its Self-Assembly with Surfactant Molecules, *Soft Matter* **2012**, *8*, 8735-8742.

(43) Dallavalle, M.; Leonzio, M.; Calvaresi, M.; Zerbetto, F. Explaining Fullerene Dispersion by using Micellar Solutions. *ChemPhysChem* **2014**, *15*, 2998-3005.

(44) Nie, S. Y.; Lin, W. J.; Yao, N.; Guo, X. D.; Zhang, L. J. Drug Release from pH-Sensitive Polymeric Micelles with Different Drug Distributions: Insight from Coarse-Grained Simulations. *ACS Appl. Mater. Interfaces* **2014**, *6*, 17668-17678.

(45) Luu, X. C.; Yu, J.; Striolo, A. Ellipsoidal Janus Nanoparticles Adsorbed at the Water−Oil Interface: Some Evidence of Emergent Behavior. *J. Phys. Chem. B* **2013**, *117*, 13922-13929.

(46) Yue, T.; Zhang, X. Cooperative Effect in Receptor-Mediated Endocytosis of Multiple Nanoparticles. *ACS Nano*, **2012**, *6*, 3196-3205.

(47) Ding, H.; Tian, W.; Ma, Y. Designing Nanoparticle Translocation through Membranes by Computer Simulations. *ACS Nano*, **2012**, *6*, 1230-1238.

(48) Masoud, H.; Alexeev, A. Controlled Release of Nanoparticles and Macromolecules from Responsive Microgel Capsules. *ACS Nano*, **2012**, *6*, 212-219.

(49) Alexeev, A.; Uspal, W. E.; Balazs, A. C. Harnessing Janus Nanoparticles to Create Controllable Pores in Membranes. *ACS Nano*, **2008**, *2*, 1117-1122.

(50) Groot, R. D.; Warren, P. B. Dissipative Particle Dynamics: Bridging the Gap Between Atomistic and Mesoscopic Simulation *J. Chem. Phys.* **1997**, *107*, 4423-4435.

(51) Groot, R. D.; Madden, T. J. Dynamic Simulation of Diblock Copolymer Microphase Separation. *J. Chem. Phys.* **1998**, *108*, 8713-8724.

(52) Culgi BV. The Netherlands. Available from: http://www.culgi.com; **2011**.

(53) Koelman, J. M. V. A.; Hoogerbrugge, P. J. Dynamic Simulation of Hard Sphere Suspensions Under Steady Shear. *Europhys. Lett.* **1993**, *21*, 363-368.

(54) Groot, R. D.; Rabone, K. L. Mesoscopic Simulation of Cell Membrane Damage, Morphology Change and Rupture by Nonionic Surfactants. *Biophys. J.* **2001**, *81*, 725-736.

(55) Partington, J. R.; Hudson, R. F.; Bagnall, K. W. Self-Diffusion of Aliphatic Alcohols. *Nature* **1952**, *169*, 583-584.

(56) Shillcock, J. C.; Lipowsky, R. Equilibrium Structure and Lateral Stress Distribution of Amphiphilic Bilayers from Dissipative Particle Dynamics Simulations. *J. Chem. Phys*. **2002**, *117*, 5048-5061.

(57) Zhang, H.; Peng, C.; Yang, J.; Lv, M.; Liu, R.; He, D.; Fan, C.; Huang, Q. Uniform Ultrasmall Graphene Oxide Nanosheets with Low Cytotoxicity and High Cellular Uptake. *ACS Appl. Mater. Interfaces* **2013**, *5*, 1761-1767.

(58) Liu, J.; Conboy, J. C. 1,2-Diacyl-Phosphatidylcholine Flip-Flop Measured Directly by Sum-Frequency Vibrational Spectroscopy. *Biophys. J.* **2005**, *89*, 2522-2532.

(59) Devaux, P. F.; Herrmann, A.; Ohlwein, N.; Kozlov, M. M. How Lipid Flippases Can Modulate Membrane Structure. *Biochim. Biophys. Acta* **2008**, *1778*, 1591–1600.

(60) Li, Y.; Liu, Y.; Fu, Y.; Wei, T.; Le Guyader, L.; Gao, G.; Liu, R.; Changb Y.; Chena, C. The Triggering of Apoptosis in Macrophages by Pristine Graphene Through the MAPK and TGF-Beta Signaling Pathways. *Biomaterials* **2012**, *33*, 402-411.

(61) Calvaresi, M.; Zerbetto, F. Baiting Proteins with C_{60}. *ACS Nano*, **2010**, *4*, 2283-2299.

(62) Zuo, G.; Huang, Q.; Wei, G.; Zhou, R.; Fang, H. Plugging into proteins: poisoning protein function by a hydrophobic nanoparticle. *ACS Nano* **2010**, *4*, 7508-7514.

(63) Calvaresi, M.; Zerbetto, F. Fullerene sorting proteins. *Nanoscale* **2011**, *3*, 2873-2881.

(64) Zuo, G.; Kang, S.-G.; Xiu, P.; Zhao, Y.; Zhou, R. Interactions Between Proteins and Carbon-Based Nanoparticles: Exploring the Origin of Nanotoxicity at the Molecular Level. *Small* **2013**, *9*, 1546-1556.

(65) Calvaresi, M.; Hoefinger, S.; Zerbetto, F. Probing the Structure of Lysozyme–Carbon-Nanotube Hybrids with Molecular Dynamics. *Chem. Eur. J.* **2012**, *18*, 4308-4313.

(66) Yang, S.-T.; Liu, Y.; Wang, Y.-W.; Cao, A. Biosafety and Bioapplication of Nanomaterials by Designing Protein–Nanoparticle Interactions. *Small* **2013**, *9*, 1635-1653.

(67) Calvaresi, M.; Zerbetto, F. The Devil and Holy Water: Protein and Carbon Nanotube Hybrids. *Acc. Chem. Res.*, **2013**, *46*, 2454-2463.

(68) Calvaresi, M.; Arnesano, F.; Bonacchi, S.; Bottoni, A.; Calo`, V.; Conte, S.; Falini, G.; Fermani S.; Losacco, M.; Montalti, M.; Natile, G.; Prodi, L.; Sparla, F.; Zerbetto, F.

C_{60}@Lysozyme: direct observation by nuclear magnetic resonance of a 1:1 fullerene protein adduct. *ACS Nano* ***2014***, *8*, 1871-1877.

(69) Sun, X.; Feng, Z.; Hou, T.; Li, Y. Mechanism of Graphene Oxide as an Enzyme Inhibitor from Molecular Dynamics Simulations. *ACS Appl. Mater. Interfaces* **2014**, *6*, 7153−7163.

(70) Luan, B.; Huynh, T.; Zhao, L.; Zhou, R. Potential Toxicity of Graphene to Cell Functions *via* Disrupting Protein–Protein Interactions. *ACS Nano*, **2014**, DOI**:** 10.1021/nn506011j

GRAPHICAL TABLE OF CONTENTS